Iranian Journal of Geophysics, Vol 20 No 6, 2027, Page 105 – 127 (Research Article)
DOI: 10.30499/ijg.2025.535052.1716

Upveiling subsurface structures of the Sarulla geothermal field of north Sumatera through satellite -based gravity modeling

Turmudi Turmudi[1*], Agustya Martha[1] andRizki Wijayanti[2]

[1] *Assistant Professor, Limnology and Water Resource Research Centre, National Research and Innovation Agency (BRIN), Indonesia*
[2] *Assistant Professor, Faculty Of Mathematics And Natural Sciences Jenderal Soedirman University, Indonesia*

(Received: 17 July 2025, Accepted: 23 November 2025)

Abstract

This study presents a comprehensive analysis of the subsurface geological structures of the Sarulla geothermal field located in North Sumatera, Indonesia, utilizing satellite-based gravity modelling techniques. The aim of this study were to: a) Identify the presence and characteristics of fault structures in the Sarulla Geothermal Field using gravity derivative analysis; b). Interpret the subsurface lithology of the geothermal system through 2D forward gravity modelling; c). Evaluate the geothermal resource potential. Employing high-resolution satellite gravity data from the GGMplus model, gravity anomaly maps were generated and interpreted through advanced modeling approaches to identify density variations indicative of subsurface features such as faults, fractures, and lithological boundaries. The methodology integrates satellite gravity data processing, anomaly separation, and forward and inverse gravity modelling to construct a detailed subsurface structural model. Key findings reveal significant gravity anomalies correlating with major tectonic structures and geothermal reservoirs, highlighting zones of enhanced permeability and heat flow. These results provide critical insights into the spatial distribution of geothermal reservoirs and the structural controls influencing fluid migration and heat accumulation. The study underscores the effectiveness of satellite gravity modelling as a non- invasive, cost-efficient tool for geothermal exploration, particularly in regions with limited ground-based geophysical data. The implications of this research extend to optimizing drilling targets, reducing exploration risks, and supporting sustainable geothermal development in the Sarulla field and similar geothermal systems worldwide. This work contributes to the growing body of knowledge on remote sensing applications in geothermal resource assessment and demonstrates the potential of integrating satellite gravity data with geological and geophysical information for enhanced subsurface characterization.

Keywords: Satellite gravity modelling, Sarulla geothermal system, gravity derivative analysis, subsurface structure interpretation, geothermal exploration

[*]Corresponding author: turm001@brin.go.id

1 Introduction

Geothermal energy stands out as a vital renewable energy source due to its sustainability, reliability, and low carbon footprint. Unlike intermittent sources such as solar and wind, geothermal energy provides a stable base-load supply, essential for supporting growing global energy demands and addressing climate change. (Eze et al., 2025);(Barasa Kabeyi & Olanrewaju, 2022). Indonesia, located on the Pacific Ring of Fire, holds the world's second-largest geothermal potential, estimated at 29 GW. Among the regions with the highest potential is North Sumatera, which hosts major geothermal fields including the Sarulla Geothermal Field (Alhusni et al., 2023).

The Sarulla field, located in North Tapanuli Regency, has an installed capacity exceeding 330 MW, making it one of the largest in Southeast Asia. It plays a critical role in Indonesia's renewable energy strategy, contributing to the government's 23% renewable energy target by 2025. Development of geothermal energy in North Sumatra also contributes to regional economic development, rural electrification, and environmental sustainability (Nukman & Hochstein, 2019).

The tectonic setting of the Sarulla area, part of the Sunda Arc, is characterized by complex subduction and volcanic processes. The geothermal system is associated with the Great Sumatera Fault, a major strike-slip fault accommodating the convergence between the Indo-Australian and Eurasian plates. The field is underlain by Quaternary volcanic rocks, including andesitic to dacitic lava flows and pyroclastic deposits (Siringoringo et al., 2024). High-enthalpy geothermal reservoirs are hosted in fractured andesite and volcanic breccias, with fluid circulation facilitated by fault and fracture networks.

Understanding the subsurface structure of the Sarulla field is essential for optimizing exploration and development strategies (Purwanto, 2019). Traditional geophysical methods, while effective, are often limited by logistical and financial constraints. Satellite-based gravity modelling offers a cost-effective alternative with wide spatial coverage and high-resolution data. This method measures variations in Earth's gravitational field caused by subsurface density differences, enabling the identification of faults, lithological boundaries, and geothermal reservoirs (Dadrass Javan et al., 2025).

This study utilizes gravity data from the GGMplus satellite model, which integrates measurements from GRACE and GOCE satellite missions. These data are processed using terrain corrections, filtering, and regional-residual separation to highlight geological features. Forward and inverse modelling techniques are applied to interpret subsurface structures and density anomalies. The approach has been successfully used in various geothermal regions, including the Taupo Volcanic Zone and East African Rift, demonstrating its reliability (Yusuf et al., 2021).

The significance of this study lies in its ability to enhance the understanding of Sarulla's complex geological framework using a non-invasive, high-resolution approach. By identifying density anomalies linked to faults and lithology, the research contributes to more accurate drilling, better reservoir management, and reduced exploration risks (Abiyudo et al., 2021);(Cao et al., 2024). Furthermore, it offers a replicable methodology for other geothermal fields facing similar challenges.

Several previous studies have investigated Sarulla's geothermal system using various methods. For example, (Afshar et al., 2023) employed gravity and magneto telluric data to map fault systems, while (Catur Wibowo & Benaya Lumban Tobing, 2022) applied gravity and seismic methods in volcanic settings. Koesuma et al., (2025) integrated satellite gravity with geological and geochemical data to assess potential geothermal zones. However, limitations in spatial resolution and modelling accuracy remain. This research addresses these gaps through advanced satellite gravity modelling and 2D forward modelling, providing a refined structural interpretation of the Sarulla geothermal system.

Objectives of the Study: (1)To identify the presence and characteristics of fault structures in the Sarulla Geothermal Field using gravity derivative analysis; (2) To interpret the subsurface lithology of the geothermal system through 2D forward gravity modelling; (3) To evaluate the geothermal resource potential in the Sarulla area, North Tapanuli Regency, North Sumatera Province.

2 Methods

2.1 Study Area and Data

This research was carried out over a period of five months, from December 2024 to April 2025. The primary dataset used in this study consists of secondary gravity data obtained from the Global Gravity Model Plus (GGMPlus), which integrates satellite-derived gravity anomalies and terrestrial measurements. The gravity dataset was accessed through the National Research and Innovation Agency (BRIN), located in Cibinong, Indonesia.

The study area covers the Sarulla Geothermal Field, situated in North Tapanuli Regency, North Sumatera Province, Indonesia. Geographically, the region is bounded by 98°54′ to 99°12′ East Longitude and 1°42′ to 2°01′ South Latitude, encompassing a broad zone of tectonic and geothermal interest. A map of the study area is presented in Figure 1, indicating the spatial extent and coordinate boundaries used in the analysis.

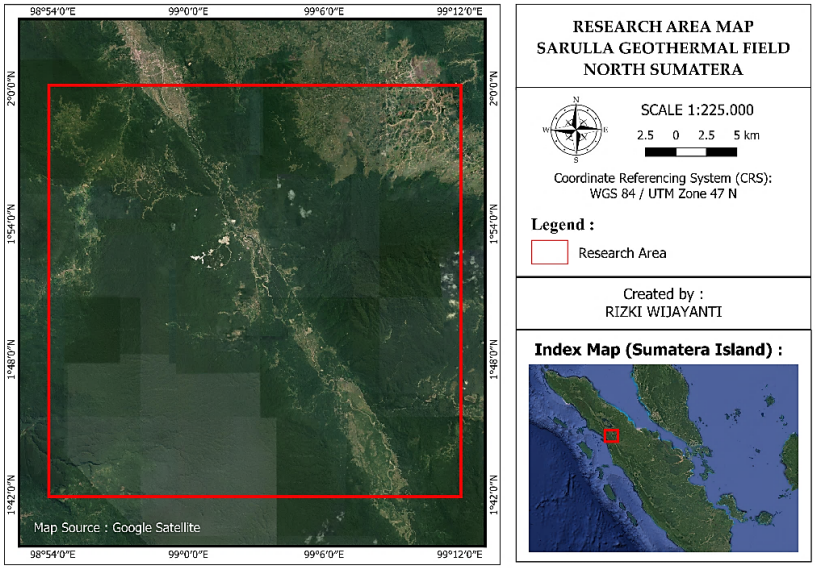

Figure.1 Study Area of Sarulla Geothermal Field North Sumatera, Indonesia.

The Sarulla Geothermal Field is situated in North Tapanuli Regency, within the province of North Sumatera, Indonesia. This region is part of the Bukit Barisan mountain range, which extends along the western spine of Sumatera and is characterized by complex tectonic and volcanic activity associated with the Sumatera Fault Zone (SFZ).

The topography is generally mountainous, with elevations ranging from moderate hills to highland terrains, contributing to a favorable geothermal gradient. The area is also influenced by a tropical rainforest climate, with high annual rainfall and dense vegetation cover.

2.2 Regional Geology of The Sarulla Geothermal Field

The island of Sumatra lies along the Sunda Trench, a northwest–southeast trending subduction zone forming the convergent boundary between the Indo-Australian oceanic plate and the Eurasian continental plate. The oblique nature of this convergence results in complex tectonic deformation, characterized by the development of the Sumatran Volcanic Arc and the Sumatera Fault System (SFS), a major dextral (right-lateral) strike-slip fault trending N30° - 40°W (Dasgupta & Mandal, 2022).

The SFS accommodates oblique convergence through lateral displacement and transtensional regimes, forming a series of segmented pull-apart basins and associated fracture networks. This structural setting promotes geothermal activity through enhanced permeability, heat flow, and magmatic intrusions (Kumari et al., 2018).

As shown in Figure 2, the lithology of the Sarulla Geothermal Field comprises both volcanic and sedimentary formations. Key stratigraphic units include:

- Alluvium Formation (Qh): Consisting of unconsolidated clay, silt, sand, and gravel deposits formed in fluvial and coastal environments.
- Toru Formation (Qpto): Characterized by tuffaceous silt and sand, indicative of pyroclastic and epiclastic processes.
- Toba Tuff Formation: Composed of rhyodacitic ignimbrites deposited by the Toba supereruption, one of the largest Quaternary volcanic events (Mucek et al., 2021).
- Toru Volcanic Rocks: Consist mainly of andesite lavas, agglomerates, and breccias, reflecting proximal volcanic deposition.
- Tapanuli Group: Includes meta- conglomerates, meta-arenites, and slates representing older basement lithologies.

This region is tectonically and volcanically active, dominated by northwest–southeast trending faults, and extensively covered by Quaternary volcanic deposits. These conditions contribute to its high geothermal prospectivity (J. Zhang et al., 2024).

Surface geothermal manifestations at Sarulla are spatially associated with fault zones and fracture systems generated by the Great Sumatera Fault. The strike-slip dextral motion of the fault has produced transtensional basins and fault intersections that act as permeable pathways for geothermal fluids (Sutrisno et al., 2019). Key manifestations include hot springs, warm springs, fumaroles, gas seeps (hot and cold), and areas of hydrothermal alteration.

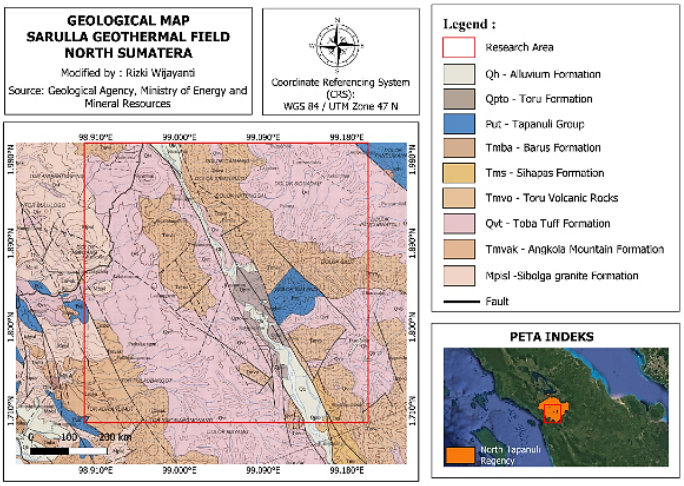

Figure 2. Geological Map of Sarulla Geothermal Field.

Geothermal manifestations in the Sarulla field are distributed across four main zones: Namora-I-Langit, Silangkitang, Donotasik, and Sibualbuali (Maulana et al., 2024). These features are aligned northwest–southeast along fault-controlled structures. The geothermal system is hosted by relatively young volcanic units (Quaternary) and locally exposed Tertiary and basement formations, with a high-enthalpy reservoir (>300 °C) located at depth (Chaudhary et al., 2025).

The regional geological framework, particularly the interaction between volcanism and faulting, plays a critical role in reservoir development, fluid migration, and heat distribution (Tavakoli & Barfizadeh, 2024). Accurate structural interpretation is thus essential for sustainable resource management and drilling optimization.

2.3 Geothermal System

Geothermal energy is a form of renewable energy derived from the natural heat of the Earth's interior, transferred to the surface primarily through conduction and convection mechanisms. Conduction occurs via thermal transmission through rocks, whereas convection involves the movement of fluids typically meteoric water that interacts with heat sources at depth. A geothermal system is defined as a natural heat transfer process occurring within a specific volume of the Earth's crust, channeling thermal energy from a deep heat source to the surface, where it manifests through various thermal expressions (Firdaus et al., 2014).

Although geothermal heat exists beneath most of the Earth's surface, viable geothermal energy resources are localized in regions with specific geological configurations, as illustrated in Figure 3.

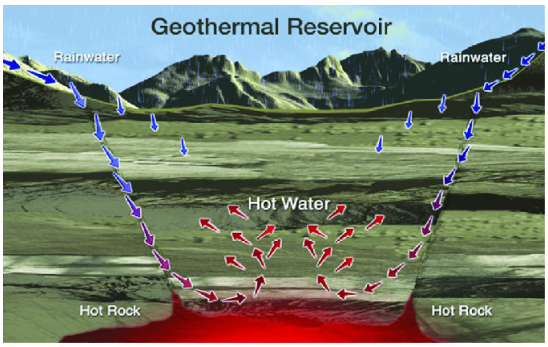

Figure 3. Model of Geothermal System (Kumar et al., 2019).

This model demonstrates how rainwater infiltrates the subsurface through

fractures and porous rock matrices, migrating downward until it encounters high-temperature rocks (Kumar et al., 2019). Upon contact, the water is heated, partially vaporized, and forms a pressurized geothermal fluid that circulates via convective processes. As fluid pressure builds, it seeks pathways such as faults and fractures to ascend, eventually discharging at the surface as geothermal manifestations hot springs, mud pools, fumaroles, or geysers (Putri et al., 2014).

According to Suharno, (2013), a geothermal system is structurally and thermally controlled by several key components: (1) a deep-seated magmatic or plutonic heat source, (2) a permeable reservoir rock capable of storing and transmitting fluids, (3) an overlying impermeable cap rock, usually composed of clay, acting as a seal, (4) geologic structures such as faults, folds, fractures, or unconformities that serve as conduits for fluid flow, and (5) a recharge area where surface water enters the subsurface system. The interplay of these elements governs the behaviour, sustainability, and potential exploitation of a geothermal system.

2.4 Gravity Method in Geothermal Exploration

The gravity method is one of the most widely applied geophysical techniques in resource exploration, tectonic studies, and natural hazard assessment. It allows for the delineation of subsurface geological formations by measuring spatial variations in the Earth's gravitational field, which arise due to heterogeneities in rock density (Liu et al., 2023). This method is particularly effective in identifying structural features such as faults, fractures, and subsurface reservoirs associated with geothermal activity. The theoretical foundation of gravity surveys is based on Newton's Law of Universal Gravitation (Figure 4), which states that the gravitational force $\vec{F}_{12}$ between two masses m_1 and m_2 separated by a distance r is proportional to the product of the masses and inversely proportional to the square of the distance (Harsita et al., 2024). The direction of the unit vector is from particle 1 to particle 2, so that the force exerted by particle 1 on particle 2 is expressed by:

$$\vec{F}_{12} = -G\frac{m_1 m_2}{r^2}\vec{r}_{12} \quad (1)$$

Where $\vec{F}_{12}$ is the force exerted by particle 1 on particle 2 and $\vec{r}_{12}$ is its value and unit vector, and the negative sign indicates that the two particles attract each other. The force exerted by particle 2 on particle 1, namely $\vec{F}_{21}$, is the same as $\vec{F}_{12}$ and so on in the opposite direction, which is in accordance with Newton's third law (Serway and Jewett, 2016).

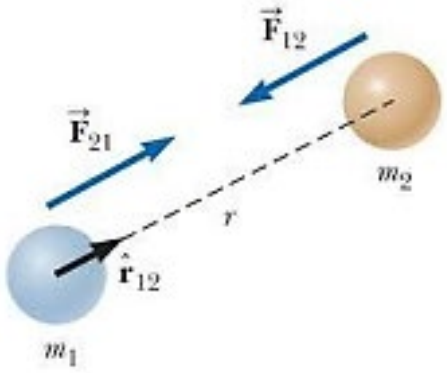

Figure 4. Gravitational force between two particles (Serway and Jewett, 2016).

2.5 GGMPlus 2013 Gravity Data

Gravity data used in geophysical studies can be acquired either through direct field measurements or obtained from satellite-derived global models. The latter approach has gained increasing importance, particularly for studies conducted in remote or data-sparse regions. Various global gravity models are now

openly accessible, such as TOPEX, BGI, EGM2008, SRTM2 and GGMPlus (Li et al., 2025), each offering different resolutions and processing techniques.

GGMPlus 2013 is an ultra-high-resolution global gravity model developed through the collaboration between Curtin University (Australia) and the Technical University of Munich (Germany). This dataset integrates satellite-based gravity data from GRACE (Gravity Recovery and Climate Experiment) and GOCE (Gravity Field and Steady-State Ocean Circulation Explorer) with the EGM2008 model to produce a refined gravity field (Nov et al., 2015). The enhancement involves the application of topographic gravity forward modelling based on spherical harmonic expansions over a geopotential reference surface, resulting in a final dataset with a resolution of approximately 7.2 arcseconds (about 200 meters in the north–south direction).

GGMPlus provides gravity disturbance values, which are physically comparable to free-air gravity anomalies and reflect deviations from a reference ellipsoidal gravity field due to mass and topographic distributions (Camacho & Alvarez, 2021). These high-resolution disturbances enable enhanced interpretation of gravity anomalies and are particularly effective in resolving subsurface geological structures.

The GGMPlus dataset has been widely used in regional geological mapping, structural analysis, and geothermal resource assessments. Its application in gravity forward or inverse modelling allows for better constraint on key geophysical parameters such as density contrast, geometry, and depth of anomalous bodies, thus improving the reliability of subsurface models (Agustin & Wibawa, 2022).

2.6 Forward Modeling of Gravity Field Data

In geophysical studies, subsurface modeling plays a crucial role in interpreting gravity anomalies and understanding the geological framework of the Earth's crust. There are two principal modeling approaches: forward modelling and inverse modelling (Blakely, 1995; Telford et al., 1990).

Forward modelling involves constructing a hypothetical subsurface model based on geological assumptions and calculating the theoretical gravity response at the surface. The model is iteratively adjusted until the calculated anomaly closely fits the observed gravity data. This approach is particularly useful when prior geological or geophysical constraints are available, providing a direct means to evaluate different subsurface scenarios (Neugebauer, 1988).

Conversely, inverse modelling works in the opposite direction—starting from the observed gravity data and using mathematical inversion techniques to estimate the parameters of the subsurface model. This data-driven method, often referred to as data fitting, seeks to minimize the misfit between measured and predicted anomalies, producing a model that best explains the observations within an acceptable error margin (Li and Oldenburg, 1998).

In this study, two-dimensional forward modeling was performed using the GM-SYS module in Geosoft Oasis Montaj software to map the subsurface geological structure of the Sarulla Geothermal Field. This approach primarily relied on residual Bouguer anomaly data. It was further supported by geological data, surface topography features, the presence of fault structures from the results of FHD and SVD analysis, and density values representing lithological units in

the study area. These density parameters were obtained from Telford et al (1990). Significant anomalous changes in body contact will cause the FHD to have a maximum value so that it can indicate the boundary of the geological structure based on gravity data. This analysis method can determine the horizontal density contrast boundary from gravity data. The first horizontal derivative (FHD) can be calculated using the following equation (Zaenudin and Yulistina, 2020).

$$FHD = \sqrt{\left(\frac{\delta g}{\delta x}\right)^2 + \left(\frac{\delta g}{\delta y}\right)^2} \quad (2)$$

Meanwhile, Second Vertical Derivative (SVD) is a gravity interpretation method that helps to indicate structures or faults. The SVD method is the second derivative value of vertical z-direction gravity field data that provides a picture of residual anomalies associated with shallow structures so that it can indicate the type of fault structure detected based on the results of the SVD data trajectory. The calculation of the Second Vertical Derivative (SVD) is carried out through the following equation (Sumintadireja et al., 2018):

$$\nabla^2 \Delta g = 0 \quad (3)$$

$$\frac{\partial^2 \Delta g}{\partial x^2} + \frac{\partial^2 \Delta g}{\partial y^2} + \frac{\partial^2 \Delta g}{\partial z^2} = 0 \quad (4)$$

$$\frac{\partial^2 \Delta g}{\partial z^2} = \left(\frac{\partial^2 \Delta g}{\partial x^2} + \frac{\partial^2 \Delta g}{\partial y^2}\right) \quad (5)$$

2.7 Tools and Material

This study utilized a range of tools and datasets to process and interpret gravity data for geothermal potential analysis in the Sarulla Geothermal Field. The selected tools supported the workflows for gravity correction, coordinate transformation, data filtering, and two-dimensional forward modelling. An overview of the tools and materials used is presented in Table 1.

2.8 Research Procedures for Gravitational Field Data Processing

This study was systematically carried out through three main phases: (1) gravity field data acquisition, (2) gravity data processing, and (3) interpretation. Each phase was designed to ensure methodological rigor and to facilitate the extraction of subsurface geological information with high reliability. (Figure 5).

3. Results and Discussion

3.1 Topography of the Sarulla Geothermal Field Derived from Gravity Field Analysis

Topography plays a fundamental role in geothermal exploration, as variations in surface elevation can reflect underlying geological structures, including faults, fractures, and volcanic features (X. Zhang et al., 2023). The topographic characteristics of the Sarulla Geothermal Field were analysed in conjunction with gravity field data to better understand the geomorphological context of the study area.

The topographic map generated from the gravity-based interpretation reveals that the Sarulla region exhibits significant variation in elevation, ranging from approximately 474.31 m to 1464.05 m above sea level (ASL). This elevation range suggests a complex terrain shaped by volcanic and tectonic processes typical of the geo- dynamical active environment of North Sumatera. (Figure 6)

High-elevation zones are predominantly associated with volcanic edifices and structural uplifts, while lower areas may correspond to sediment-filled depressions or erosion-controlled valleys. These topographic patterns not only reflect the surface morphology but may

also correlate with subsurface density contrasts captured in the gravity anomaly data, further supporting structural interpretation.(Dumais & Brönner, 2020).

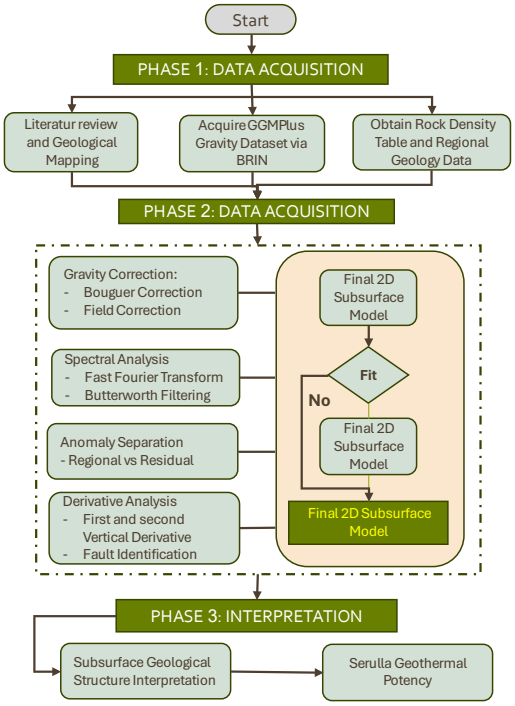

Figure 5. Flowchart Of Reseach Activity.

Table 1. Tools and materials used in the study

No.	Tool/Material	Description
1	**Microsoft Excel 2019**	Used for gravity correction calculations (free-air, Bouguer, terrain), computation of Complete Bouguer Anomaly (CBA), depth estimation graphs, and preparation of input data for filtering and modeling.
2	**Notepad++**	Utilized for formatting corrected gravity data into ASCII format (*.txt) compatible with Geosoft Oasis Montaj.
3	**Google Earth Pro**	Used to define the coordinate boundaries of the study area based on high-resolution satellite imagery (Google, 2024).
4	**Surfer 25** (Golden Software)	Applied to convert geographical coordinates (latitude/longitude) into Universal Transverse Mercator (UTM) projection for spatial analysis.
5	**Global Mapper v24**	Employed to extract Digital Elevation Models (DEM) and clip them according to research boundaries for terrain correction and regional-residual analysis.
6	**Geosoft Oasis Montaj 2020**	Main software platform for gravity data processing, including gridding, regional-residual separation, First Horizontal Derivative (FHD), Second Vertical Derivative (SVD), and 2D forward modeling using the GM-SYS module (Geosoft, 2020).
7	**QGIS 3.34 LTR**	Open-source GIS software used to compile, digitize, and visualize geological and structural maps of the research area (QGIS Development Team, 2024).
8	**Laptop Computer**	Lenovo Ideapad equipped with Intel® Core™ i3-1005G1 processor, 4 GB RAM, used to run all software tools listed above.
9	**GGMPlus Gravity Dataset**	Secondary gravity dataset from the Global Gravity Model Plus (GGMPlus), providing terrain-corrected gravity anomalies and corresponding DEM data (Hirt et al., 2013).
10	**Geological Map**	Geological base map of the research area obtained from the Geological Agency, Ministry of Energy and Mineral Resources (ESDM), Indonesia (ESDM, 2020).

The integration of topographic and gravity field data provides valuable insights into the spatial distribution of geothermal features and contributes to a more accurate delineation of potential reservoir zones within the Sarulla Geothermal Field.(Kremer et al., 2025); (Purwanto, 2019)

This topographic variation not only reflects the geological complexity of the Sarulla Geothermal Field but also plays a critical role in influencing surface hydrology, geothermal gradient distribution, and structural control on fluid pathways.

The topography of the Sarulla Geothermal Field, as illustrated in Figure 6, reveals a complex elevation profile indicative of tectonic and volcanic influences. The study area can be morphologically divided into three distinct topographic zones:

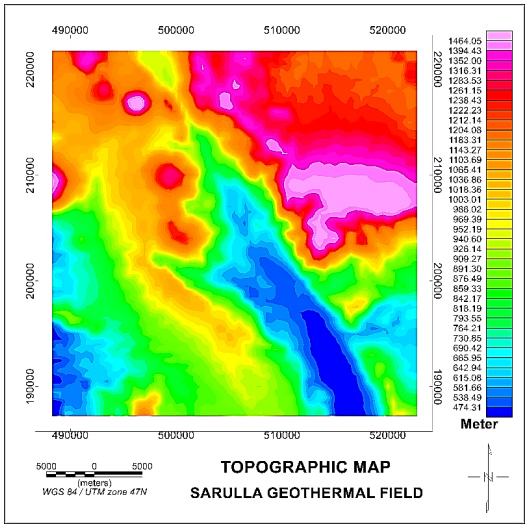

Figure 6. Topographic Map of Sarulla Geothermal Field.

1). Highland Zone

This zone is located predominantly in the northwestern, northeastern, and eastern parts of the study area. Elevations in this region range from 1316.31 to 1464.05 m ASL, represented by light to dark purple hues. These elevated areas likely correspond to volcanic edifices or uplifted structural blocks, which may serve as recharge zones in the geothermal system.

2). Hilly Terrain

Covering the central and transitional zones, this area exhibits elevations between 764.21 and 1283.53 m ASL, shown in green to red colours. This region is characterized by moderate relief and undulating terrain, potentially reflecting erosional surfaces or tilted fault blocks influenced by extensional tectonics.

3). Lowland Zone

The southern, southeastern, and southwestern parts of the field consist of relatively flat to gently sloping terrain, with elevations ranging from 474.31 to 690.42 m ASL, depicted in blue tones. These areas are hypothesized to be tectonic depressions or sedimentary basins that may function as discharge zones for geothermal fluids.

The spatial distribution of these topographic units provides critical context for interpreting the geothermal system's structural control and hydrothermal pathways. Notably, the alignment of elevation gradients appears to follow a northwest–southeast trend, consistent with regional fault patterns identified in previous structural studies.

3.2 Complete Bouguer Gravity Anomaly

The Complete Bouguer Anomaly (CBA) represents the final gravity anomaly obtained after applying a series of corrections including drift, tidal, latitude, free-air, and Bouguer slab corrections to the observed gravity data. The resulting values are then interpolated using a gridding algorithm to generate the Complete Bouguer Anomaly map (Figure 7). The similarity between the topographic map

and the Complete Bouguer Anomaly (CBA) map indicates the influence of surface relief on the gravitational response in the study area. To avoid biased interpretations due to uncompensated topographic effects, terrain correction was applied using GGMplus Digital Elevation Model (DEM) data. The corrected Bouguer anomalies were then integrated with Bouguer correction and free-air correction, resulting in a more accurate and representative CBA map. This approach effectively reduces the dominance of topographic influences. Therefore, the similarity of patterns between topographic maps and CBA essentially indicates the control of geological structures over surface morphology, rather than the influence from uncorrected topography. Although this map provides a clearer representation of the gravitational field, it still contains a degree of non-uniqueness or ambiguity, as the anomalies represent integrated effects from both shallow and deep-seated geological structures. This can complicate direct interpretation of specific subsurface features without further modelling. As shown in Figure 7, the Complete Bouguer Anomaly values in the study area range from –17.58 mGal to 41.75 mGal, illustrated using a color gradient from dark.
blue (low anomaly) to light pink (high anomaly). These variations reflect the spatial heterogeneity of rock mass density in the subsurface, which is influenced by lithology, structure, and the presence of geothermal reservoirs or intrusions. The gravity anomaly distribution can be broadly classified into three anomaly zones:

1). Low Anomaly Zone (–17.58 to 23.43 mGal)

Depicted by dark blue to light green hues, this zone is predominantly concentrated in the central part of the study area, with minor occurrences in the southeastern sector, corresponding spatially to the known Sarulla Geothermal Field. The low anomaly suggests the presence of low-density materials, which may be associated with altered volcanic rocks, sedimentary infill, or geothermal fluid accumulation.

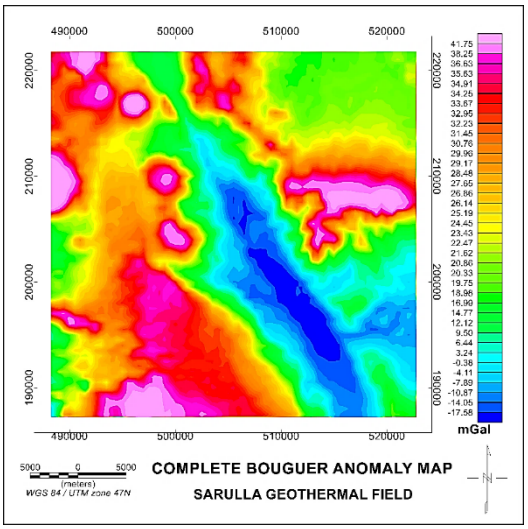

Figure 7. Complete Bouguer Gravity Field Anomaly Map.

2). Moderate Anomaly Zone (24.45 to 31.45 mGal)

Represented by yellow to orange tones, these values are distributed across the western, eastern, and northern margins of the study area. This intermediate anomaly range is likely indicative of transitional lithologies, such as fractured and partially altered volcanic rocks, or regions influenced by faulting and moderate density contrasts.

3). High Anomaly Zone (32.23 to 41.75 mGal)

Marked by red to light purple colours, high anomaly values are observed in the eastern, northwestern, and southwestern parts of the study area. These zones may be associated with the presence of dense igneous intrusions, crystalline basement highs, or structurally uplifted blocks.
The spatial pattern of gravity anomalies

reveals important insights into the subsurface geological architecture, especially when integrated with topographic and geological data. Notably, the central low-anomaly zone coincides with the geothermal field, suggesting a potential correlation between low-density zones and hydrothermal alteration or fluid presence.

3.3 Spectrum Analysis of Gravity Field Anomalies

To estimate the depth of subsurface structures, spectral analysis was performed using the Radially Averaged Power Spectrum (RAPS) method. This approach enables the decomposition of gravity field anomalies into components associated with different depth sources (Mondal et al., 2020). The spectral curve, as illustrated in Figure 8, consists of three main segments representing regional anomalies, residual anomalies, and noise, each corresponding to distinct frequency domains.

The analytical process involves transforming the gravity anomaly data into the frequency domain and plotting the logarithm of the power spectrum (LnP) against the radial frequency (CYC/K_Unit). In this context, long-wavelength, low-frequency components (blue segment) represent regional anomalies typically sourced from deep geological structures. Conversely, short-wavelength, high-frequency components (red segment) reflect residual anomalies, which are generally associated with shallow features such as faults, volcanic bodies, or sedimentary layering. The noise component (green segment) comprises very high-frequency data and is usually not related to geological structures (Yang et al., 2020).

By fitting linear regression lines to each segment of the spectrum, slope values (gradients) were obtained from which depth estimates were calculated using the spectral depth formula (Maiti et al., 2020):

$$depth = \frac{slope}{4\pi} \quad (6)$$

The results of this depth estimation are summarized in Table 2.

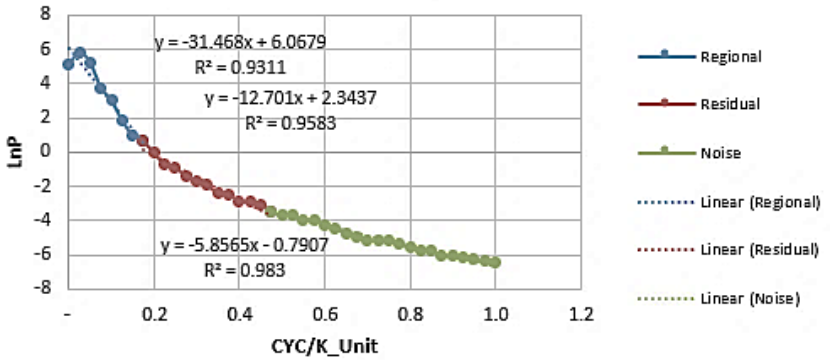

Figure 8. Spectrum Analysis in Microsoft Excel.

Table 2. Estimated Depth of Subsurface.

Component	Slope	Estimated Depth (km)	R^2
Regional	31.468	2.50	0.9311
Regional	12.701	1.01	0.9583
Noise	5.856	0.47	0.983

Sources Based on Spectral Analysis.

The regional component exhibits the steepest slope (31.468) and corresponds to a depth of approximately 2.50 km, indicating the influence of deeper geological features such as basement topography or intrusive bodies. The residual anomaly segment, with a slope of 12.701, yields an estimated depth of 1.01 km, suggesting the presence of relatively shallow subsurface structures, possibly related to geothermal reservoirs or fault zones. The noise component, with the lowest slope (5.856), is interpreted as shallow surface-level interference and is not considered geologically significant. The high coefficient of determination (R^2 values > 0.93) for all segments indicates good linear fits, confirming the reliability of the spectral analysis in delineating the vertical distribution of density contrasts within the study area.(Price et al., 2023).

3.4 Regional and Residual Gravity Field Anomaly Map

The complete Bouguer anomaly represents a superposition of gravity signals originating from various depths, including deep-seated regional structures and shallow subsurface features. Therefore, spectral decomposition is required to isolate these components for a more focused geological interpretation (Kremer et al., 2025).

Based on the spectrum analysis illustrated in Figure 9, anomaly boundaries were identified using Radially Averaged Power Spectrum (RAPS) analysis. The application of a Butterworth filter with a central wavelength of approximately 8330 m and a filter degree of 24 enabled the effective separation of regional and residual components (Figure 9). This filtering process was conducted interactively to ensure accurate partitioning of long-wavelength regional signals and short-wavelength residual features (Mohandesi, 2023).

Figure 10 presents the regional gravity anomaly map, where values range from approximately –18.00 to 39.74 mGal. This map reveals broad, smooth anomaly patterns that reflect deep lithological variations and large-scale tectonic structures. Low anomaly zones, characterized by dark blue to light green hues (–18.00 to 23.37 mGal), are predominantly distributed in the central and southeastern sectors of the study area. Medium anomaly values (24.40 to 30.62 mGal), marked by yellow to orange colours, are located primarily in the western, eastern, and northern regions. High anomaly values (32.31 to 39.74 mGal), indicated by red to light purple, are concentrated in the eastern, northwestern, and southwestern margins. These variations may be associated with regional crustal thickening or denser intrusive bodies at depth.

Conversely, Figure 11 shows the residual gravity anomaly map, characterized by higher frequency and more irregular contour patterns due to its sensitivity to shallow subsurface heterogeneities. Residual anomaly values range from –8.91 to 11.42 mGal, and their distribution is indicative of more localized features such as faults, fractures, or lithological contacts. Low residual values (–8.91 to –0.74 mGal), visualized with blue to green shades, dominate the central, southeastern, and northwestern zones, with minor occurrences in the western margin. Medium anomaly values (0.50 to 2.78 mGal), displayed in yellow to orange, are evident in the western and northeastern sectors. High residual anomalies (3.21 to 11.42 mGal), marked by red to light purple, are scattered and possibly correlated with shallow dense rock bodies or fault intersections.

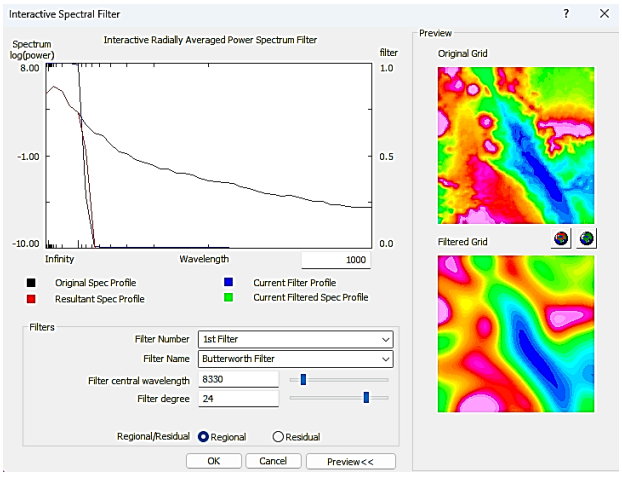

Figure 9. Separation Process of Regional and Residual Gravity Field Anomalies through Butterworth Filter.

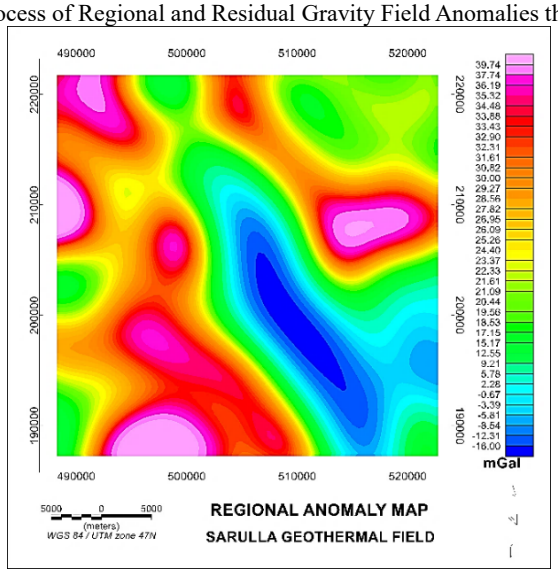

Figure 10. Regional Gravity Field Anomaly Map.

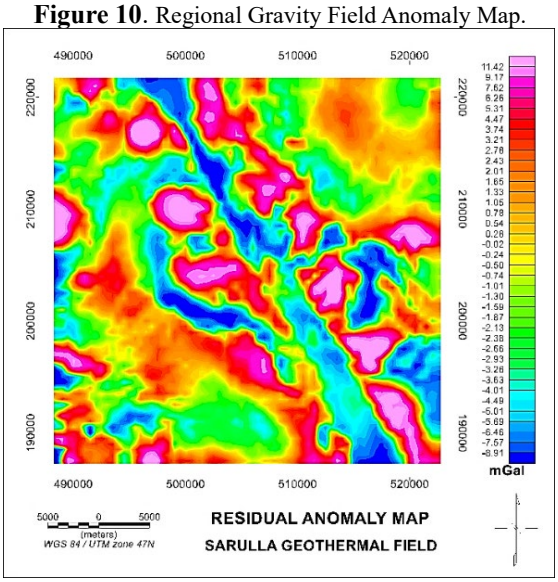

Figure 11. Residual Gravity Field Anomaly Map.

The contrast between regional and residual anomaly maps emphasizes the importance of spectral filtering in gravity studies (Xu et al., 2009). While regional anomalies provide insight into deep-seated geological frameworks, residual anomalies are instrumental in delineating near-surface structures, particularly in geothermal exploration contexts such as the Sarulla Geothermal Field.

3.5 Derivative Analysis of the Sarulla Geothermal Field Based on Gravity Data

Derivative analysis was carried out in this study to delineate the presence and pattern of fault structures controlling the Sarulla geothermal system. Two main derivative techniques were applied to the residual Bouguer anomaly map: the First Horizontal Derivative (FHD) and the Second Vertical Derivative (SVD). These methods are widely used in gravity interpretation to enhance the contrast of subsurface density boundaries and to aid structural interpretation. (Zaky & Bilqis, 2022); (Blakely, 1995; Telford et al., 1990).

The FHD method was applied to identify the edges or boundaries of density contrast associated with geological structures. In this method, fault structures are inferred from linear features with maximum FHD values, which indicate sharp lateral changes in subsurface density. As shown in Figure 12, the high anomaly values are represented by light purple shades, while black lines indicate interpreted fault traces. These fault traces predominantly appear in the central part of the study area and are consistent with the known geological fault zones as mapped in the regional geological map.

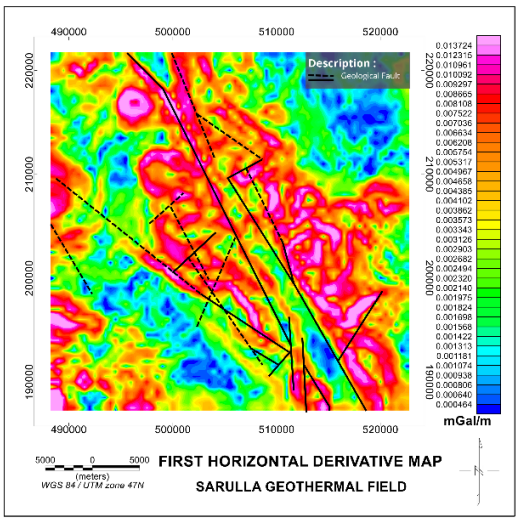

Figure 12. First Horizontal Derivative (FHD) Map.

To enhance and validate the fault delineation from the FHD, the Second Vertical Derivative (SVD) method was subsequently employed. The SVD technique enhances high-frequency signals, thereby allowing for better resolution of shallow subsurface structures (Zhu et al., 2023). The SVD map was generated using Equation (5) through the second derivative filtering function in Geosoft Oasis Montaj software. In this analysis, fault locations are inferred from zero crossings in the SVD values, which correspond to the transition zones between high and low anomaly values (Dobrin & Savit, 1988).

Figure 13 displays the SVD results, where interpreted fault structures are again indicated by black lines. These lines are located along the colour transitions between high (positive) and low (negative) anomaly zones. The correlation between FHD and SVD interpretations confirms the presence of major structural features controlling geothermal manifestations in the area.

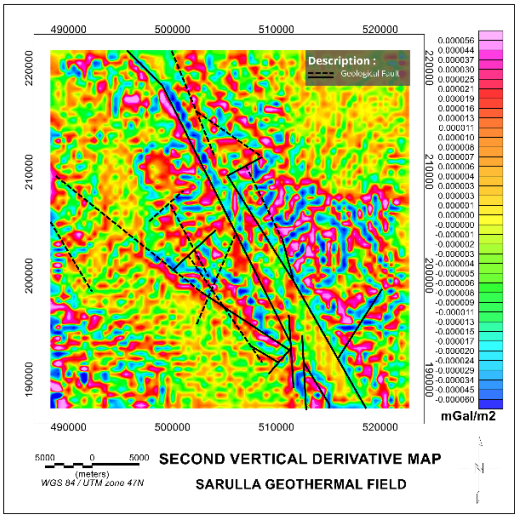

Figure 13. Second Vertical Derivative (SVD) Map.

3.6 Fault Structure Analysis

The analysis of fault structures in the Sarulla Geothermal Field was carried out through gridded digitization on both the First Horizontal Derivative (FHD) and Second Vertical Derivative (SVD) maps to delineate the geometry and type of faulting in the study area. This approach is widely adopted in gravity-based structural interpretation for geothermal exploration (Reynolds, 1997; Blakely, 1995). Three transects A–A′, B–B′, and C–C′ were drawn in a southwest–northeast direction, as shown in Figures 14 and 15. These transects are oriented perpendicularly to the dominant fault direction indicated by the regional geological map, which trends northwest–southeast around the geothermal surface manifestations.

For each transect, FHD and SVD values were extracted along Universal Transverse Mercator (UTM) coordinates (X and Y). The extracted data were plotted to generate correlation graphs between FHD and SVD values to verify the presence and type of fault structures. In this analysis, fault locations are identified by the coincidence of FHD maxima and SVD zero-crossings, indicating zones of strong lateral density contrast and vertical inflection points in the gravity field, respectively.

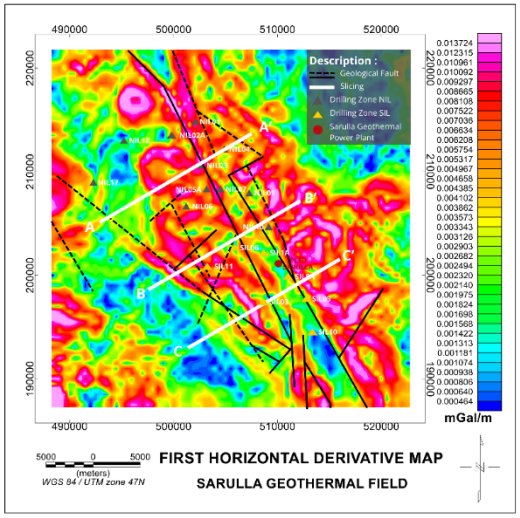

Figure 14. Slicing on the FHD Map.

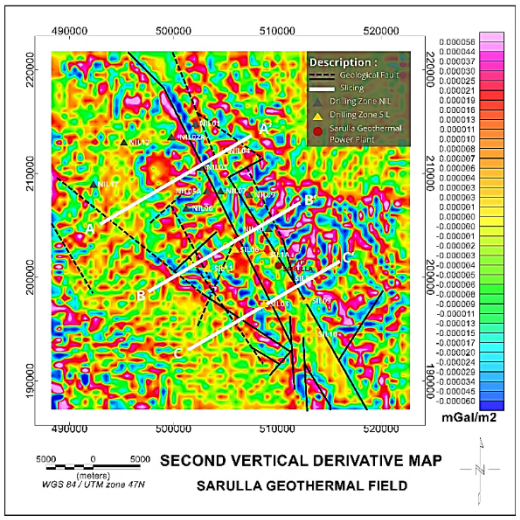

Figure 15. Slicing on the SVD Map.

In each graph, the x-axis represents the UTM X coordinate, while the y-axis displays the FHD and SVD values. The comparative trends between FHD and SVD confirm the presence of fault zones. Based on the graphical analysis, linear patterns of anomaly discontinuity highlighted with black lines indicate the interpreted fault positions.

The number of identified faults in each

transect is as follows:

- **Transect A–A′:** Three faults identified, consisting of two normal faults and one reverse fault.
- **Transect B–B′:** Four faults identified, including three normal faults and one reverse fault.
- **Transect C–C′:** Four faults identified, comprising three normal faults and one reverse fault.

The classification of fault types was based on the relative position and correlation of peak FHD values and the absolute difference between minimum and maximum SVD values. This method allows for distinguishing between normal and reverse fault behaviour based on the relative density contrast distribution and vertical deflection signatures (Rosid & Siregar, 2017).

The results are summarized in **Table 3**, which presents the coordinates and interpreted types of the fault segments. Fault locations were further visualized in Figures 16 and 17. A total of 11 fault points were identified in the study area, where black-coloured symbols represent reverse faults and white-coloured symbols represent normal faults. Black lines indicate fault traces from the geological map.

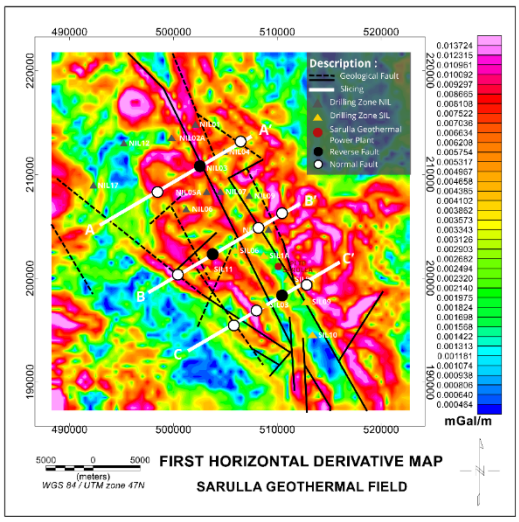

Figure 16. Plot Fault Points on the FHD Map.

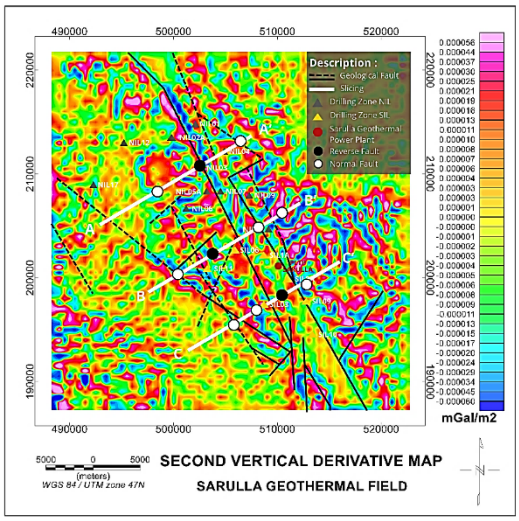

Figure 17. Plot Fault Points on the SVD Map.

Table 3. Types of Faults on Lines A, B, and C.

Section	Fault	UTM X	SVD Max	SVD Min	Jenis Patahan
A-A’	F1	498138.6	1.90E-05	-1.80E-05	Normal Fault
	F2	502677.9	3.30E-05	-1.04E-04	Reverse Fault
	F3	506344.2	2.40E-05	-1.10E-05	Normal Fault
B-B’	F4	500067.5	3.50E-05	-2.60E-05	Normal Fault
	F5	503519.2	3.20E-05	-3.50E-05	Reverse Fault
	F6	506453.8	2.10E-05	-1.10E-05	Normal Fault
	F7	510078.5	2.00E-05	-8.00E-06	Normal Fault
C-C’	F8	505754.5	1.70E-05	-1.30E-05	Normal Fault
	F9	507819.5	3.90E-05	-1.70E-05	Normal Fault
	F10	5100556.6	7.00E-06	-2.10E-06	Reverse Fault
	F11	512465.8	3.30E-05	-2.80E-05	Normal Fault

The comparison of derivative-based interpretation with geological mapping shows a strong spatial correlation, especially around the geothermal manifestation zone. The faults identified in proximity to the hot spring locations are interpreted as key conduits for geothermal fluid migration. These structures likely serve as fluid pathways controlling the surface appearance of geothermal manifestations in the area.

3.7 Results of 2D Forward Modelling of Gravity Anomaly Data

In this stage, two-dimensional (2D) forward modelling was applied to delineate the subsurface geological structures of the study area. The modelling was conducted along three profiles oriented from the southwest to the northeast, based on the residual gravity anomaly map. The average depth of modelling was constrained by prior spectral analysis. The objective was to characterize lithological variations and fault structures that may control the geothermal system in the region.

3.7.1 Profile A–A′

As shown in Figure 18, the forward model along profile A–A′ reveals a three-layer geological configuration with a modelling error of 0.95%. The uppermost layer, characterized by a low density of 1.8 g/cc, is interpreted as a caprock unit composed of altered sedimentary materials such as fluvial and coastal clays, silts, sands, and gravels. This unit is tentatively associated with the Alluvium Formation (Qh).

Beneath this, a layer with a density of 2.4 g/cc corresponds to the Toba Tuff Formation (Qvt), which is composed of pyroclastic deposits such as volcanic ash, crystals, and pumice. This layer is interpreted as the potential reservoir rock capable of storing and transmitting geothermal fluids.

The deepest layer, with a density of 2.8 g/cc, is attributed to the Toru Volcanic Formation (Tmvo), consisting of andesite, agglomerates, and breccias of volcanic origin. Structurally, this profile reveals three major faults: F1 and F3, which are interpreted as normal (extensional) faults, and F2, identified as a reverse (compressional) fault.

3.7.2 Profile B–B′

The 2D model along profile B–B′ (Figure 19) also displays a three-layered structure. The comparison of derivative-based interpretation with geological mapping shows a strong spatial correlation, especially around the geothermal manifestation zone. The faults identified in proximity to the hot spring locations are interpreted as key conduits for geothermal fluid migration (Wu & Zhou, 2023). These structures likely serve as fluid pathways controlling the surface appearance of geothermal manifestations in the area. with a slightly higher modeling error of 0.975%. The uppermost unit, with a density of 1.9 g/cc, is interpreted as the Toru Formation (Qpto), consisting of altered tuffs, diatomaceous sands, and siltstones, forming the impermeable caprock.

The intermediate layer (2.4 g/cc) is again interpreted as the geothermal reservoir zone, represented by the Toba Tuff Formation (Qvt). The bottom layer, with a density of 2.8 g/cc, corresponds to the Toru Volcanic Formation (Tmvo), composed of consolidated volcanic rocks such as andesite and volcanic breccia. Four major fault zones are identified: F4, F6, and F7 are interpreted as normal faults, suggesting extensional tectonic

regimes, while F5 is interpreted as a reverse fault, indicating localized compressive forces.

3.7.3 Profile C–C′

In contrast to the previous profiles, the forward model along profile C–C′ (Figure 20) reveals a more complex subsurface with four distinct lithological layers and a modeling error of 0.975%. The uppermost The second unit, with a density of 2.4 g/cc, corresponds to the Toba Tuff Formation (Qvt), again serving as the reservoir rock. The deepest layer, with a density of 2.7 g/cc, is interpreted as a metasedimentary unit, possibly part of the Tapanuli Group (Put), consisting of meta conglomerates, phyllites, and metaarenites.

unit exhibits variable densities ranging from 1.9 to 2.0 g/cc, representing a composite of the Toru Volcanic Formation (Tmvo) and Alluvium Formation (Qh), both acting as caprock with mixed lithologies including altered tuff, diatomaceous sands, clays, and gravels.

Beneath this, a layer with a density of 2.4 g/cc corresponds to the Toba Tuff Formation (Qvt), which is composed of pyroclastic deposits such as volcanic ash, crystals, and pumice. This layer is interpreted as the potential reservoir rock capable of storing and transmitting geothermal fluids.

The deepest layer, with a density of 2.8 g/cc, is attributed to the Toru Volcanic Formation (Tmvo), consisting of andesite, agglomerates, and breccias of volcanic origin. Structurally, this profile reveals three major faults: F1 and F3, which are interpreted as normal (extensional) faults, and F2, identified as a reverse (compressional) fault.

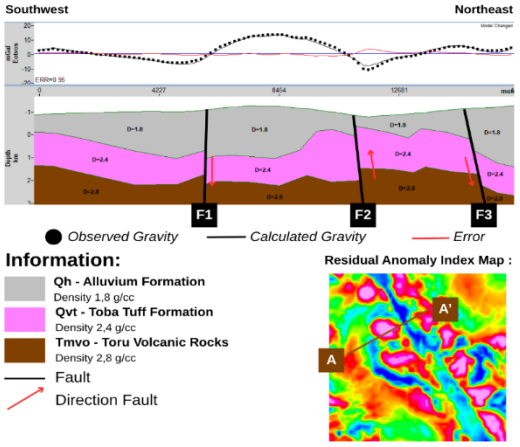

Figure 18. Forward Modelling 2D section A-A'.

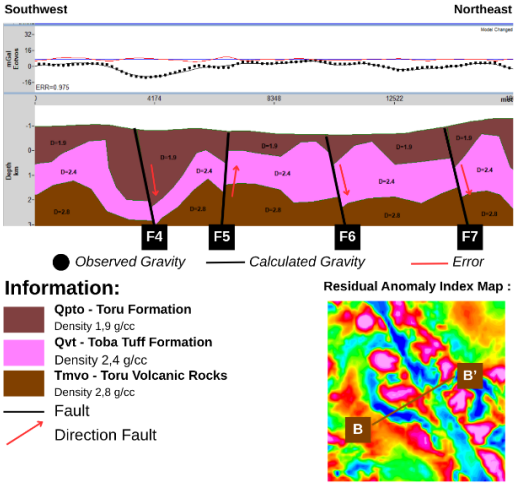

Figure 19. Forward Modelling 2D Section B-B'

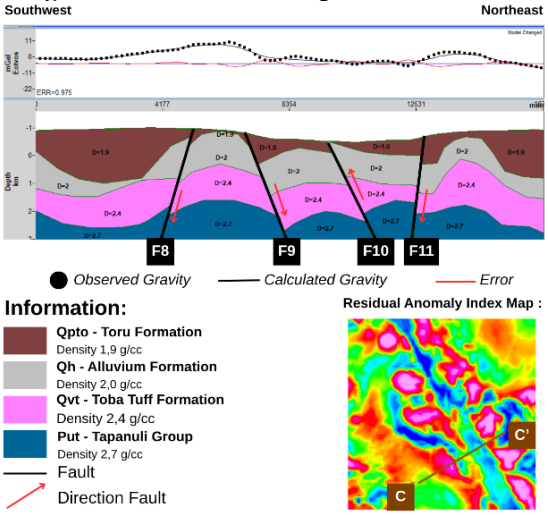

Figure 20. Forward Modelling 2D Section C-C'

4 Conclusion

Based on the results of gravity-based geophysical investigations conducted in the Sarulla Geothermal Field, several key conclusions regarding the subsurface geological structure and geothermal potential of the area can be drawn:

a. Fault Structure Analysis

Derivative-based analysis of gravity data successfully identified two major types of fault structures within the study area. Along profile A–A', two normal faults and one reverse fault were interpreted. Similarly, three normal faults and one reverse fault were delineated along profile B–B', while profile C–C' revealed the presence of three normal faults and one reverse fault. These fault systems are interpreted to play a significant role in controlling the geothermal fluid pathways and are consistent with regional tectonic settings.

b. Subsurface Lithology from 2D Forward Gravity Modelling.

The results of 2D forward gravity modeling, when integrated with regional geological data, indicate that the subsurface lithology of the Sarulla Geothermal Field comprises several distinct geological formations. The caprock is interpreted to consist of clay-alteration zones, likely associated with the Young Alluvium Formation and Totolan Formation. Beneath this layer, the reservoir rocks are predominantly volcanic in origin, including andesite and volcanic breccia, interpreted as parts of the Toba Tuff Formation and Toru Volcanic Complex. These lithological units are consistent with the geothermal system framework commonly observed in volcanic-hosted geothermal fields.

c. Geothermal Resource Potential

The Sarulla Geothermal Field exhibits significant geothermal resource potential, as evidenced by the widespread occurrence of surface manifestations and fault-controlled structures, which act as conduits for hydrothermal fluid migration. The presence of a subsurface reservoir composed of volcanic rocks, particularly andesite and volcanic breccia, further supports the geothermal viability of the area. Based on these findings, it is recommended that the identified high-potential zones be considered for further exploration and development, including additional drilling targets. Such measures would enhance the sustainable utilization of geothermal resources in the Sarulla field over the long term.

References

Abiyudo, R., Yunus, D., & Satya, D. Y. (2021). Subsurface Structure Identification from Gravity Modelling of Silangkitang. *PROCEEDINGS, The 2nd Digital Indonesia International Geothermal Convention (DIIGC) 2021*, *September*.

Afshar, A., Norouzi, G. H., & Moradzadeh, A. (2023). Exploring Geothermal Potential through Multi-Modal Geophysical Data Integration: Gravity, Magnetic, and Magnetotelluric Prospecting. *International Journal of Mining and Geo-Engineering*, *57*(4), 427–434. https://doi.org/10.22059/ijmge.2023.364057.595093

Agustin, N., & Wibawa, A. (2022). Analisis Data Gravitasi Untuk Identifikasi Struktur Bawah Permukaan Daerah Potensi Panas Bumi Cipari. *Jambura Geoscience Review*, *4*(1), 22–32. https://doi.org/10.34312/jgeosrev.v4i1.12114

Alhusni, H., Satria, T., Perdana, P., Purwanto, E. H., & Setyawan, H. (2023). Geothermal Business Outlook in Indonesia. *48th Workshop on Geothermal Reservoir Engineering Stanford University*, *2021*, 1–12. https://pangea.stanford.edu/ERE/db/GeoConf/papers/SGW/2023/Habibi.pdf

Barasa Kabeyi, M. J., & Olanrewaju, O. A. (2022). Geothermal wellhead technology power plants in grid electricity generation: A

review. *Energy Strategy Reviews*, *39*. https://doi.org/10.1016/j.esr.2021.100735

Camacho, M., & Alvarez, R. (2021). Geophysical Modeling with Satellite Gravity Data: Eigen-6C4 vs. GGM Plus. *Engineering*, *13*(12), 690–706. https://doi.org/10.4236/eng.2021.1312050

Cao, X., Liu, Z., Hu, C., Song, X., Quaye, J. A., & Lu, N. (2024). Three-Dimensional Geological Modelling in Earth Science Research: An In-Depth Review and Perspective Analysis. *Minerals*, *14*(7). https://doi.org/10.3390/min14070686

Catur Wibowo, R., & Benaya Lumban Tobing, J. (2022). Geological Structure Identification using Derivative Analysis of Gravity Method. *JIT Journal of Innovation and Technology*, *3*(2), 2721–8570. https://doi.org/10.31629/jit.v3i2.5048

Chaudhary, P., Mohan, K., Singh, D., Sumer, K., Ramdayal, C., & Prabhjot, S. (2025). Characterization of the geothermal zone by remote sensing , hydrochemical , and magnetotellurics data : a case study from Lasundra , Gujarat , India. *Acta Geophysica*. https://doi.org/10.1007/s11600-025-01636-z

Dadrass Javan, F., Samadzadegan, F., Toosi, A., & van der Meijde, M. (2025). Unmanned Aerial Geophysical Remote Sensing: A Systematic Review. *Remote Sensing*, *17*(1). https://doi.org/10.3390/rs17010110

Dasgupta, R., & Mandal, N. (2022). Role of double-subduction dynamics in the topographic evolution of the Sunda Plate. *Geophysical Journal International*, *230*(1), 696–713. https://doi.org/10.1093/gji/ggac025

Dumais, M. A., & Brönner, M. (2020). Revisiting Austfonna, Svalbard, with potential field methods - A new characterization of the bed topography and its physical properties. *Cryosphere*, *14*(1), 183–197. https://doi.org/10.5194/tc-14-183-2020

Eze, V. H. U., Eze, E. C., Alaneme, G. U., & Bubu, P. E. (2025). Recent progress and emerging technologies in geothermal energy utilization for sustainable building heating and cooling: a focus on smart system integration and enhanced efficiency solutions. *Frontiers in Built Environment*, *11*(June), 1–22. https://doi.org/10.3389/fbuil.2025.1594355

Firdaus, A., Harmoko, U., & Widada, S. (2014). Pemodelan Steady State Sistem Panas Bumi Daerah Sumber Air Panas Diwak-Derakan Dengan Menggunakan Software Hydrothrm 2.2. *Younger Physics Journal*, *3*(4), 243–250.

Koesuma, S., Sanjaya, A. S., & Nuryani, N. (2025). Identification of geothermal energy sources using gravity method (Satellite Gravimetry) in the Mount Lawu Area. *Journal of Physics: Conference Series*, *2945*(1). https://doi.org/10.1088/1742-6596/2945/1/012030

Kremer, T., Ars, J. M., Gaubert-Bastide, T., Khazraj, K., & Voisin, C. (2025). Chapter 6 • The use of passive seismic methods for Geothermal exploration and monitoring. In *Geophysics in geothermal exploration: a review*. https://doi.org/10.1051/978-2-7598-3752-6.c006

Kumar, S., Gupta, S. K., & Rawat, M. (2019). Resources and utilization of geothermal energy in India: An Eco - friendly approach towards sustainability. *Materials Today: Proceedings*, *26*(March), 1660–1665. https://doi.org/10.1016/j.matpr.2020.02.347

Kumari, W. G. P., Ranjith, P. G., Perera, M. S. A., & Chen, B. K. (2018). Experimental investigation of quenching effect on mechanical, microstructural and flow characteristics of reservoir rocks: Thermal stimulation method for geothermal energy extraction. *Journal of Petroleum Science and Engineering*, *162*(September 2017), 419–433. https://doi.org/10.1016/j.petrol.2017.12.033

Li, W., Yang, F., Zuo, X., He, C., Zhao, D., & Zhang, K. (2025). An Important Monitoring Technology for Near-Earth Space Environment—Ionospheric Tomography: Evolution, Challenges, Application and Perspectives. *Space Science Reviews*, *221*(5). https://doi.org/10.1007/s11214-025-01179-1

Liu, J., Li, S., Jiang, S., Wang, X., & Zhang, J. (2023). Tools for Edge Detection of Gravity Data: Comparison and Application to Tectonic Boundary Mapping in the Molucca Sea. *Surveys in Geophysics*, *44*(6), 1781–1810. https://doi.org/10.1007/s10712-023-09784-x

Maiti, S., Ravi Kumar, C., Sarkar, P., Tiwari, R. K., & Srinu, U. (2020). Interface depth modelling of gravity data and altitude variations: a Bayesian neural network approach. *Neural Computing and Applications*, *32*(8), 3183–3202. https://doi.org/10.1007/s00521-019-04276-9

Maulana, Y., Saepuloh, A., & Fattah, E. I. (2024). Ground displacement analysis in the

Sarulla geothermal field using Persistent Scatterer Interferometric Synthetic Aperture Radar (PS-InSAR) method. *IOP Conference Series: Earth and Environmental Science*, *1293*(1). https://doi.org/10.1088/1755-1315/1293/1/012006

Mohandesi, A. (2023). *Characteristics of Topside Equatorial Ionospheric Irregularities : An Investigation Using Swarm Echo Measurements*.

Mondal, S., Srivastava, S., & Gupta, A. K. (2020). Interpretation of resistivity data using 3D Euler deconvolution and Radially Averaged Power Spectrum. *Journal of Earth System Science*, *129*(1). https://doi.org/10.1007/s12040-020-1345-9

Mucek, A. E., Danišík, M., de Silva, S. L., Miggins, D. P., Schmitt, A. K., Pratomo, I., Koppers, A., & Gillespie, J. (2021). Resurgence initiation and subsolidus eruption of cold carapace of warm magma at Toba Caldera, Sumatra. *Communications Earth and Environment*, *2*(1). https://doi.org/10.1038/s43247-021-00260-1

Neugebauer, M. (1988). Reviews of Geophysics. *Eos, Transactions American Geophysical Union*, *69*(37), 849–849. https://doi.org/10.1029/88EO01108

Nov, P. P., Republic, C., President, V., Crespi, M., Group, J. S., Multiresolutional, H. G., Committee, T. I., … Assembly, I. X. (2015). *Inter-Commission Committee on Theory (ICCT)*. 1–75.

Nukman, M., & Hochstein, M. P. (2019). The Sipoholon Geothermal Field and adjacent geothermal systems along the North-Central Sumatra Fault Belt, Indonesia: Reviews on geochemistry, tectonics, and natural heat loss. *Journal of Asian Earth Sciences*, *170*(October 2018), 316–328. https://doi.org/10.1016/j.jseaes.2018.11.007

Price, J., Sousa, D., & Sousa, F. J. (2023). Effect of Spatial and Spectral Scaling on Joint Characterization of the Spectral Mixture Residual: Comparative Analysis of AVIRIS and WorldView-3 SWIR for Geologic Mapping in Anza-Borrego Desert State Park. *Sensors*, *23*(15). https://doi.org/10.3390/s23156742

Purwanto, E. H. (2019). Assessment of exploration strategies, results and costs of geothermal fields in Indonesia. *Unu-Gtp*, *September*, 1–34.

Putri, M. K., Suharno, & Hidayatika, A. (2014). Introduction to Geothermal System of Way Ratai. *Proceedings Indonesia International Geothermal Convention & Exhibition*, *September*, 1–5. http://repository.lppm.unila.ac.id/52052/1/Introduction to Geothermal System of Way Ratai.pdf

Rosid, M. S., & Siregar, H. (2017). Determining fault structure using first horizontal derivative (FHD) and horizontal vertical diagonal maxima (HVDM) method: A comparative study. *AIP Conference Proceedings*, *1862*(July). https://doi.org/10.1063/1.4991275

Siringoringo, L. P., Sapiie, B., Rudyawan, A., & Sucipta, I. G. B. E. (2024). Origin of high heat flow in the back-arc basins of Sumatra: An opportunity for geothermal energy development. *Energy Geoscience*, *5*(3), 100289. https://doi.org/10.1016/j.engeos.2024.100289

Suharno. (2013). *BukuEsplorasiGeothermalSUHARNO*. *1*.

Sumintadireja, P., Dahrin, D., & Grandis, H. (2018). A note on the use of the second vertical derivative (SVD) of gravity data with reference to Indonesian cases. *Journal of Engineering and Technological Sciences*, *50*(1), 127–139. https://doi.org/10.5614/j.eng.technol.sci.2018.50.1.9

Sutrisno, L., Bonte, D., Daud, Y., Smit, J., Beekman, F., Wees, J. D. Van, & Purwanto, W. (2019). Assessing the Role of Pull-Apart Basins for High-Temperature Geothermal Resources in Transcurrent Tectonic Setting: Sumatra and California Compared. *European Geothermal Congress*, *June*, 1–8.

Tavakoli, V., & Barfizadeh, H. (2024). The role of plate movements on reservoir development of the Iranian carbonate formations: A review of the interplay between tectonics, paleoclimate, and diagenesis. *Results in Earth Sciences*, *2*(April), 100037. https://doi.org/10.1016/j.rines.2024.100037

Wu, Y., & Zhou, X. (2023). Structural control effects on hot springs' hydrochemistry in the northern Red River Fault Zone: Implications for geothermal systems in fault zones. *Journal of Hydrology*, *623*(February), 129836. https://doi.org/10.1016/j.jhydrol.2023.129836

Xu, Y., Hao, T., Li, Z., Duan, Q., & Zhang, L.

(2009). Regional gravity anomaly separation using wavelet transform and spectrum analysis. *Journal of Geophysics and Engineering*, *6*(3), 279–287. https://doi.org/10.1088/1742-2132/6/3/007

Yang, Y., Liu, C., & Langston, C. A. (2020). Processing seismic ambient noise data with the continuous wavelet transform to obtain reliable empirical Green's functions. *Geophysical Journal International*, *222*(2), 1224–1235. https://doi.org/10.1093/gji/ggaa243

Yusuf, A., San, L. H., & Abir, I. A. (2021). A preliminary geothermal prospectivity mapping based on integrated GIS, remote-sensing, and geophysical techniques around northeastern Nigeria. *Sustainability (Switzerland)*, *13*(15). https://doi.org/10.3390/su13158525

Zaky, D. A., & Bilqis, A. (2022). Application of Generalized Derivative Operator on Bouguer Anomaly for Detecting Geological Structures. *JGE (Jurnal Geofisika Eksplorasi)*, *8*(2), 113–126. https://doi.org/10.23960/jge.v8i2.204

Zhang, J., Chen, L., Sun, Y., Xu, L., Zhao, X., Li, Q., & Zhang, D. (2024). Geothermal resource distribution and prospects for development and utilization in China. *Natural Gas Industry B*, *11*(1), 6–18. https://doi.org/10.1016/j.ngib.2024.01.001

Zhang, X., Zhang, Y., Li, Y., Huang, Y., Zhao, J., Yi, Y., Li, J., Zhang, J., & Zhang, D. (2023). Geothermal Spatial Potential and Distribution Assessment Using a Hierarchical Structure Model Combining GIS, Remote Sensing, and Geophysical Techniques—A Case Study of Dali's Eryuan Area. *Energies*, *16*(18). https://doi.org/10.3390/en16186530

Zhu, Q., Sui, L., Li, Q., Li, Y., Gu, L., & Wang, D. (2023). The Single-Channel Microseismic Mine Signal Denoising Method and Application Based on Frequency Domain Singular Value Decomposition (FSVD). *Sustainability (Switzerland)*, *15*(13). https://doi.org/10.3390/su151310588.